

Comparison of Filters for Despeckle With Improved Speckle Reducing Anisotropic Diffusion Filter for Ultrasound Images

^[1] Stafford Michahial, ^[2] Dr Bindu A Thomas
^[1] Associate Proffesor Dept. of EEE ^[2] Prof & Head, Dept. of ECE
^[1] GSSS Institute of Engineering & Technology for Women, Mysore
^[2] Vidya Vikas Institute of Engineering & Technology

Abstract: ---- Due to the presence of speckle noise leads to the poor quality of the US images. The presence of speckle noise makes it difficult to understand the information contain in the US image hence filtering of US image is required to improve the image quality. The paper gives us the comparison of different filters techniques (linear filter (lf), Anisotropic Diffusion(AD), Nonlinear filter kuwahara(Kuwa) ,median filter(med),hybrid median filter(hmed) , Lee Filter & kaun, frost filter, Wavelet based speckle reduction methods, speckle reducing anisotropic diffusion filter (srad),improved srad(Israd). 65 texture feature, image intensity normalization, 15 image quantitative metrics and image quality evaluation. It is observed that the Israd, improves the image quality of liver, kidney, uterus, live mass ultrasound images.

I. INTRODUCTION

In recent years there is a lot of advancement and progress in image processing however, a lot of factors in the image quality, hinders the automated image analysis [1], and diseases evaluation [2]. This includes artifacts by image acquisition instrumentations, transmission errors, coding artifacts, which will degrade the image quality and induce noise in ultrasound image. Cancer is the most deadly disease in both men and women there are several types of cancer like lung cancer, Prostrate cancer, Breast Cancer, Uterus Cancer etc these diseases can cause of death Hence diagnosis of the cancer in the early stages is crucial. Ultrasound imaging is a widely used technology for diagnosing and treatment of cancer. Noninvasive methods used to diagnose cancer still have limitations. Detection techniques are currently based primarily on physical examination. Ultrasound image segmentation is an important problem in medical image analysis and visualization. Because these images contain strong speckle noise and attenuation artifacts [3], it is difficult to automatically segment these images to detect interested objects in the correct position and orientation. The Fig. 1 gives the flowchart analysis of ultrasound image analysis used in the paper to compare 10 different filtering techniques

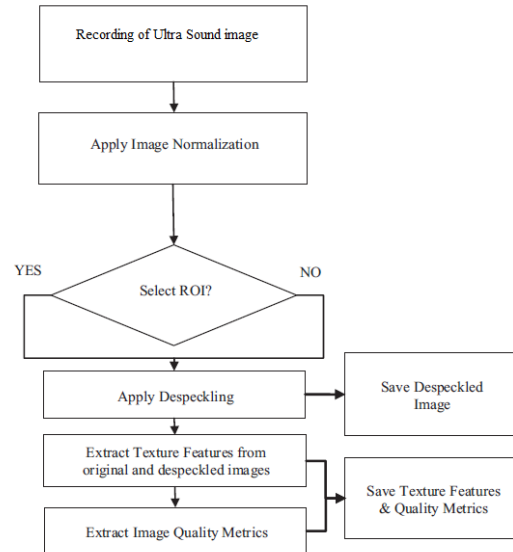


Fig. 1 – Flowchart analysis of the for ultrasound Image analysis

In order to analysis the performance of the different filters 50 ultra sound images of liver, uterus, breast, and kidney.

II. SPECKLE FILTERS

In this section,10 image despeckle filtering methods are presented as follows: (a) linear filter,(b) Anisotropic

**International Journal of Engineering Research in Electronic and Communication Engineering
(IJERCE)
Vol 3, Issue 5, May 2016**

Diffusion (c) nonlinear filterkuwahara , (d) median filter, (e) hybrid median filter , (f) Lee Filter&kaun, and (g) frost filter (h) Wavelet based speckle reduction methods (i) speckle reducing anisotropic diffusion filter (srad), (j) improved srad.

(a) Linear despeckle filter

This filters uses 1st order statistics mean, variance of neighboring pixel that is described by the multiplicative noise model [4,5,26]. The algorithms based on the equations given below:

$$f_{i,j} = \bar{g} + k_{i,j}(g_{i,j} - \bar{g})$$

$g_{i,j}$, $k_{i,j}$ is a weighting factor, where $k \in [0, 1]$, and i, j are the pixel coordinates. The factor $k_{i,j}$, is a function of the local statistics in a moving window and is defined by the equation:

$$k_{i,j} = \frac{1 - g^{-2}\sigma^2}{\sigma^2 + \sigma_n^2}$$

The values σ^2 represent the variance of the moving window and σ_n^2 the variance of noise in the whole image. The noise variance can be calculated from the logarithmically compressed image by computing the average noise variance over a number of windows with dimensions considerably larger than the filtering window. The moving window size for the despeckle filter in this study was 5×5 and the number of iterations applied to each image was two. The filter is the most appropriate in increasing the optical perception evaluation in ultrasound images and videos, while the mean and the median values are preserved in ultrasound images [5] and videos [19] by increasing the optical perception evaluation. The filter decreases the variance of speckle noise in the image, improves statistical and texture features extraction, increases the classification accuracy and the overall image quality of the image by enhancing edges [4].

(b) Anisotropic diffusion filter

Perona and Malik [31] introduced the following function, $d_{i,j,t} = f(|\nabla g|)$, that smoothed the original image while trying to preserve brightness discontinuities:

$$\frac{dg_{i,j,t}}{dt} = \text{div}[dg_{i,j,t} \nabla g_{i,j,t}] = \left[\frac{d}{dt} dg_{i,j,t} \frac{d}{dt} g_{i,j,t} \right] + \left[\frac{d}{dj} dg_{i,j,t} \frac{d}{dj} g_{i,j,t} \right]$$

Where $(|\nabla g|)$, is the gradient magnitude, and $d(|\nabla g|)$, is an edge stopping function, which is chosen to satisfy $d \rightarrow 0$ when $|\nabla g| \rightarrow \infty$ so that the diffusion is stopped across edges. This function, called the diffusion coefficient, $cd(|\nabla g|)$, is a monotonically decreasing function of the gradient magnitude, $|\nabla g|$ yielding intra-region smoothing, and not inter-region smoothing [4,5,17,27,31] by impeding diffusion at image edges. A basic anisotropic partial-differential equation is given in (5). Two different diffusion coefficients were proposed in [31], as follows:

$$cd(|\nabla g|) = \frac{1}{1 + \left(\frac{|\nabla g_{i,j}|}{K}\right)^2} \quad \text{and} \quad cd(|\nabla g|) = \frac{2|\nabla g_{i,j}|}{2 + \left(\frac{|\nabla g_{i,j}|}{K1}\right)^2}$$

where K and $K1$, are positive gradient threshold parameters, known as diffusion or flow constants [31]. In this work we used the first diffusion coefficient in (6) as it was found to perform better in our images [4,5].

(c) Nonlinear despeckle filter

The kuwahara is an 1D filter operating in a 5×5 pixel neighborhood searching for the most homogenous neighborhood area around each pixel [4, 28]. The middle pixel of the 1×5 neighborhood is then substituted by the median gray level of the 1×5 mask. The filter is iteratively applied to the image where the number of iterations is selected by the user. In this study the number of iterations selected for the despeckle filter kuwahara was set to two. The kuwahara filter can be used to improve the classification accuracy of different organs and tissues and to enhance edges, thus also improving the optical perception evaluation [3].

(d) Median , hybrid median despeckle filters

The filter median [4,5] is a median filter applied over windows of size 5×5 . This is an extension of the filter hmedian, which was introduced in [30] and later used in [4,5] and it computes the median of the outputs generated by median filtering with three different windows (cross shape window, x-shape window and normal window). The moving size window for the despeckle filter median and hmedian was for both filters 5×5 pixels, while the number of iterations applied to each image was three and two respectively. The median filter is well suited for improving the optical perception evaluation but repeated application destroys the image edges. The filter hmedian preserves the edges and

**International Journal of Engineering Research in Electronic and Communication Engineering
(IJERECE)
Vol 3, Issue 5, May 2016**

increases the optical perception evaluation. It can thus be used to preserve and enhance edges of various organs in ultrasound images [3,4].

(f) Lee Filter and Kaun

The Lee filter is designed to eliminate speckle noise while preserving edges and point features in radar imagery. Based on a linear speckle noise model and the minimum mean square error (MMSE) design approach. Lee filter form an output image by computing a linear combination of the center pixel intensity in a filter window with the average intensity of the window. Kaun and Lee filter have the same formulation although signal model assumption and derivations are different. These two filters achieve a balance between straight forward averaging in homogeneous regions and identity filter where edges and point features exist. This balance depends on the coefficient of variation inside the moving window.

(g) Frost Filter

Frost achieves a balance between averaging and all pass filter by forming an exponentially shaped filter kernel. The response of the filter varies locally with the coefficient of variation

(h) Wavelet based speckle reduction methods

The wavelet based speckle reduction method usually includes (1) logarithmic transformation (2) wavelet transformation (3) modification of noisy coefficient using shrinkage function (4) invert wavelet transform and (5) exponential transformation. This method can be classified into three groups

1. Thresholding methods - The wavelet coefficients smaller than the predefined threshold are regarded as contributed by noise and then removed [19],[20]. The thresholding techniques have difficulty in determining an appropriate threshold.
2. Bayesian estimation methods - This Method approximates the noise free signal based on the distribution model of noise free signal and that of noise [21]-[23]. Thus, reasonable distribution models are crucial to the successful application of these techniques to medical ultrasound imaging

3. Coefficients correlation methods - This is an undecimated or over complete wavelet domain denoising method which utilizes the correlation of useful wavelet coefficients across scales [24].

However this method does not rely on the exact prior knowledge of the noise distribution and this method is more flexible and robust compared to other wavelet based methods.

III. PROPOSED FILTER IMPROVED SPECKLE REDUCING ANISOTROPIC DIFFUSION FILTER (ISRAD)

Due to noise and speckles in the ultrasound B mode and elastographic images, noise filtering and edge-enhancement are required. There are several fundamental requirements of noise filtering methods for medical images. One, it should not lose the important information of object boundaries and detailed structures. Two, it should efficiently remove noise in the homogeneous regions and finally, it should enhance morphological definition by sharpening discontinuities. The Speckle Reducing Anisotropic Diffusion (SRAD) filter (Yongjian Yu and T. Scott Acton, 2002) meets these requirements of noise filters and also improves the image quality significantly while preserving the important boundary information and hence, in present study, speckle reducing anisotropic diffusion filtering of real elastography and ultrasound B mode images is done to reduce noise and speckles. Segmentation is required to separate the tumor region from its background. Improved Speckle reducing anisotropic diffusion proposed is Based on setting the diffusion coefficient in the diffusion equation using the local frame gradient and the frame Laplacian. The Israd filter uses two seemingly different methods, namely the Lee [26] and the Frost diffusion filters [27]. In [33], a more general updated function for the output image is presented, by extending the PDE versions of the despeckle filter as:

$$f_{i,j} = g_{i,j} + \frac{1}{\eta_s} \text{div}(c_{srad}(|\nabla g|) \nabla g_{i,j})$$

where η_s is the size of the filtering window. The diffusion coefficient for the speckle anisotropic diffusion, $c_{srad}(|\nabla g|)$ is given in [33] as:

**International Journal of Engineering Research in Electronic and Communication Engineering
(IJERECE)
Vol 3, Issue 5, May 2016**

Table 2: Spatial gray level dependence matrices

$$c_{srad}^2(|\nabla g|) = \frac{(1/2)|\nabla g_{i,j}|^2 - (1/16)(\nabla^2 g_{i,j})^2}{(g_{i,j} + (1/4)\nabla^2 g_{i,j})^2}$$

It is required that $c_{srad}(|\nabla g|) \geq 0$. The above instantaneous coefficient of variation combines a normalized gradient magnitude operator and a normalized Laplacian operator to act like an edge detector. High relative gradient magnitude and low relative Laplacian indicates an edge. The Israd filter utilizes speckle reducing anisotropic diffusion according to (12) with the diffusion coefficient, $c_{srad}(|\nabla g|)$ in (13) [33]. The coefficient of variation for the Israd filter can be selected from 0.01 up to 0.1 and the number of iterations from 1 to 200. In this study the number of iterations applied to each image, was set to 30, while the coefficient of variation was 0.02. As it was observed during the processing the Israd filter may be used to improve the overall image quality. It was furthermore observed to improve the quality of video encoding as well reducing the bandwidth required for transmitting the filtered ultrasound image over a 3G wireless network [32].

Results and conclusion



Fig 1: Ultra sound image of kidney

Table 1: statistical features

	Original	Linear despeckle	Anisotropic diffusion filter	kuvshinov	Median	hybrid median	Lee	Kaun	Frost	SRAD	ISRAD
Mean	33.96	36.422	38.2843	34.66	33.67	33.73	41.5	21.52	38.09	40.8010	33.96
Median	6.483	26.355	14.1151	5.312	6.147	6.10	11.99	0	11.98	12.75	6.483
Std.Dev	46.32	71.93	49.4468	47.8	45.70	45.74	55.0	40.33	48.23	52.8085	46.32
Skewness	1.615	1.361	1.59937	1.600	1.589	1.58	1.4	2.149	1.38	1.56929	1.615
Kurtosis	5.733	3.872	5.60787	5.417	5.64	5.6	4.5	7.5	4.5	5.57659	5.733

	Original	Linear despeckle	Anisotropic diffusion filter	kuvshinov	Median	hybrid median	Lee	Kaun	Frost	SRAD	ISRAD
Angular 2nd moment	0.0920	0.0711	0.0569	0.0963	0.0979	0.0908	0.077	0.3258	0.0701	0.0569	0.0920
Contrast	284.9046	126.804	1321.262	455.66	228.23	240.32	230.87	206.31	109.78	240.28	284.90
Correlation	0.931347	0.986720	0.722368	0.89439	0.943908	0.9409	0.9564	0.93452	0.9751	0.9500	0.9313
Variance	2081.756	4818.0702	2383.656	2171.583	2042.543	2043.072	2694.4	1580.592	2218.6	2451.2	2081.7
Inverse difference moment	0.485263	0.461363	0.40147054	0.556921	0.578343	0.556157	0.51908	0.709791	0.5411	0.4595	0.4852
sum average	69.4013	110.09146	78.0730034	69.86559	68.99766	69.0729	80.4025	44.24617	76.806	80.348	69.401
sum variance	8042.12	19145.476	8213.36533	8230.871	7941.939	7931.961	10546.9	6116.037	8764.9	9564.6	8042.1
sum entropy	4.342812	4.6296596	4.71348987	4.291004	4.30639	4.333623	4.27213	2.97441	4.5315	4.6225	4.3428
Entropy	6.085541	6.222768	6.97090400	5.811362	5.772807	5.843587	5.96207	3.889825	5.9505	6.3874	6.0855
difference variance	254.0477	92.774937	1116.54326	422.7219	211.8193	221.8208	209.866	193.4373	91.469	209.11	254.04
difference entropy	2.425104	2.5092255	3.0947148	2.195095	2.065076	2.120986	2.20381	1.611279	2.1445	2.4759	2.4251
correlation -1	-0.39107	-0.475619	-0.2911209	-0.44744	-0.47322	-0.45699	-0.4849	-0.32004	-0.5105	-0.4019	-0.3910
correlation -2	0.97206	0.9892292	0.95010107	0.981242	0.983354	0.983095	0.98838	0.966219	0.9911	0.9800	0.9720

Table 3: gray level difference statistics

	Original	Linear despeckle	Anisotropic diffusion filter	kuvshinov	Median	hybrid median	Lee	Kaun	Frost	SRAD	ISRAD
Angular 2nd moment	0.010776	0.0045242	0.007963745	0.00828	0.005711	0.009579	0.00459	0.007722	0.003509	0.009417	0.0107
Contrast	243.0795	94.184517	671.6543379	347.5428	212.2073	223.9016	154.7836	203.4296	80.2091	238.7137	243.07
Correlation	0.059411	0.0104659	0.144959145	0.084082	0.052799	0.053723	0.032663	0.063542	0.018911	0.051916	0.0594
Variance	54.36199	270.78999	32.01902545	95.71983	31.69703	34.37309	254.8036	29.86297	78.37458	288.0812	54.36
Inverse difference moment	0.081142	0.1344081	0.081176405	0.091469	0.06718	0.104178	0.09992	0.056751	0.088065	0.08665	0.0811
sum average	0.319947	3.5775982	0.332648314	1.101815	0.491038	0.520875	3.502041	0.605048	0.990071	2.75043	0.3199
sum variance	449.1696	1177.3445	839.3009533	750.4221	417.3548	436.619	1173.197	322.8814	395.7074	1311.039	449.16
sum entropy	0.041064	0.0215229	0.05885253	0.031895	0.027914	0.036596	0.01237	0.027207	0.018562	0.036146	0.0410
Entropy	0.348233	0.3198289	0.324493856	0.376933	0.317475	0.394322	0.343537	0.234923	0.335246	0.317943	0.3482
difference variance	217.7681	58.020145	526.0829785	313.6238	198.3218	206.5268	136.2055	188.2647	61.30584	208.5125	217.76
difference entropy	0.425727	0.3791396	0.418136517	0.465913	0.364606	0.469385	0.485476	0.349308	0.451546	0.413257	0.4257
correlation -1	0.093217	0.0812018	0.080556503	0.10443	0.084927	0.105014	0.091862	0.093621	0.08868	0.084336	0.0932
correlation -2	0.018608	0.0067337	0.031743651	0.013806	0.009051	0.012703	0.008022	0.016239	0.005898	0.013001	0.0186
Contrast	284.7906	126.60875	1320.980633	455.4486	228.1324	240.2313	230.509	206.1873	109.7384	239.9468	284.79
Angular 2nd moment	0.18668	0.1706031	0.129638738	0.23969	0.26348	0.241415	0.210603	0.226626	0.226913	0.167857	0.186
Entropy	2.43341	2.5246071	3.10218374	2.204366	2.071248	2.130886	2.214832	1.617837	2.154018	2.483645	2.433
Mean	5.428846	5.6400222	14.13272207	3.56421	3.965245	4.180272	4.441924	3.449804	4.132563	5.456383	5.4288

Table 4: Gray level difference statistics

	Original	Linear despeckle	Anisotropic diffusion filter	kuvshinov	Median	hybrid median	Lee	Kaun	Frost	SRAD	ISRAD
coarseness	10.293	18.2024	3.05723	3.68301	27.703	21.295	39.561	4.3667	54.370	13.85526	10.293
contrast	0.2373	0.27609	0.79606	0.2159	0.1428	0.1745	0.1463	0.0687	0.0592	0.226589	0.2373
busyness	1.31E-5	3.946E-6	4.30149E-5	3.78E-5	4.8E-06	6.22E-6	3.12E-6	4.84E-5	2.12E-5	9.81E-06	1.31E-5
complexity	134680	75795	403234.368	132393	82609	99905.4	72857.6	60040.3	34399.1	78837.31	134680
strength	2139264	3630910.9	714301.3251	2293433	3481381	2850576	3500151	6199416	8251736	2152456	2139264
coarseness	9.6206	7.41916	5.0419069	9.5216	10.906	10.873	9.5878	13.030	9.69786	7.576691	9.6206
contrast	23.87067	15.925137	51.40549877	30.1881	21.36515	21.92384	21.48848	20.31314	14.81809	21.92206	23.87067
periodicity	0.593231	0.7164176	0.452735215	0.636365	0.665427	0.661461	0.701078	0.743632	0.717575	0.713487	0.593231
roughness	2.34237	2.196551	2.670691839	2.353658	2.187517	2.202703	2.210066	2.238024	2.14982	2.183054	2.34237

Table 1, 2, 3,4 presents the results of selected texture features extracted from the entire original and the despeckled images and from an ROI (-/-), that was selected, showing significance difference after despeckle filtering ($p < 0.05$). The features were extracted from all 100 ultrasound images of the Kidney investigated in this study. These features were the median, variance (SF feature group), sum average (SGLDM range of values feature group), contrast (GLDM feature group), coarseness, busyness (NGTDM feature group), roughness (SFM feature group), energy LL kernel (LTEM feature group), Hoerst coefficient H1 (FD feature group) and angular sum (FPS feature group). It is

**International Journal of Engineering Research in Electronic and Communication Engineering
(IJERECE)
Vol 3, Issue 5, May 2016**

observed from Table 1 that almost all filters preserve the median and reduce the variance. Furthermore, it is also observed that when the Israd filters are applied to the ROI of image, they increase contrast, H1 and angular sum, but lower roughness while at the same time they preserve the rest of the features. The results of this study can also be favorably compared with the results presented in [5,12], where similar texture features values were computed for Kidney.

Table 5: Image Quality

	GAE	MSE	SNR	PSNR	MM3	MM4	UQI	SSI	AD	SC	MD	LMSE	NAE
Linear despeckle	29580.65	20.96	21.6991	24.41	38.84	53.99	0.871	0.915	-1.681	1.010	214	0.921203	0.044263
Anisotropic diffusion filter	29580.65	20.5227	22.969	23.9182	43.298	62.10	0.663	0.708	-2.45	0.988	255	4.439	0.043
Kovachava	29580.6	21.63	20.18690	25.03	41.86	62.73	0.771	0.859	-0.77	0.992	255	1.161	0.035
Median	29580.65	34.88397	4.38109	38.30946	11.0351	21.1239	0.9303	0.9722	0.141	1.001	255	0.2695	0.0086
hybrid median	29580.65	39.10678	2.694969	42.33003	6.45047	11.9208	0.9621	0.9850	0.114	1.001	145	0.0703	0.0052
Lee	29580.65	26.26541	11.74001	39.74773	19.2362	25.40716	0.8781	0.9285	1.565	1.028	175	0.3790	0.0395
Kan	29580.65	0.775936	163.7838	6.835683	189.534	204.042	0.4844	0.549	105.062	11.669	255	1.9962	0.8423
Frost	29580.65	24.76565	14.0042	28.21594	24.7109	34.0377	0.8166	0.8941	0.02513	1.013	175	1.0386	0.0328
SRAD	29580.65	2.27372	149.1601	7.6680	174.006	189.51	0.0509	0.2375	74.6270	3.709	0.258	255	1.0580
ISRAD	29580.65	1000000	0	1000000	0	0	1	1	0	1	0	0	0

Table 5 tabulates selected image quality metrics between original and despeckled images when filtering is applied on the entire image and when applied in an ROI (-/-). For all filters investigated, when filtering was applied on the entire image or in an ROI the geometric average error (GAE) was 0. This can be attributed to the fact that the information between the original and the processed images remains unchanged. The quality metrics LMSE, and NAE showed a similar performance as the MSE and RMSE whereas for the Israd filter, smaller values of the same metrics were observed.

REFERENCES

- [1] Z. Wang, A. Bovik, H. Sheikh, E. Simoncelli, Image quality assessment: from error measurement to structural similarity, *IEEE Trans. Image Process.* 13 (4) (2004) 600–612.
- [2] T. Elatrozy, A. Nicolaides, T. Tegos, A. Zarka, M. Griffin, M. Sabetai, The effect of B-mode ultrasonic image standardization of the echodensity of symptomatic and asymptomatic carotid bifurcation plaque, *Int. Angiol.* 17 (3)(1998) 179–186.
- [3] C.P. Loizou, *Ultrasound Image Analysis of the Carotid Artery, Applications in Ultrasound Filtering, Segmentation and Texture Analysis*, Lambert Academic Publishing GmbH & Co.KG, Saarbruecken, Germany, 2012.
- [4] C.P. Loizou, C.S. Pattichis, *Despeckle Filtering Algorithms and Software for Ultrasound Imaging. Synthesis Lectures on Algorithms and Software for Engineering*, Morgan & Claypool Publishers, San Rafael, CA, USA, 2008.
- [5] C.P. Loizou, C.S. Pattichis, C.I. Christodoulou, R.S.H. Istepanian, M. Pantziaris, A.N. Nicolaides, Comparative evaluation of despeckle filtering in ultrasound imaging of the carotid artery, *IEEE Trans. Ultrason. Ferroelectr. Freq. Control* 52 (2) (2005) 1653–1669.
- [6] C.M. Wu, Y.C. Chen, K.-S. Hsieh, Texture features for classification of ultrasonic images, *IEEE Trans. Med. Imaging* 11 (1992) 141–152.
- [7] C.I. Christodoulou, C.S. Pattichis, M. Pantziaris, A.N. Nicolaides, Texture-based classification of atherosclerotic carotid plaques, *IEEE Trans. Med. Imaging* 22 (7) (2003) 902–912.
- [8] R.M. Haralick, K. Shanmugam, I. Dinstein, Texture features for image classification, *IEEE Trans. Syst. Man Cybernet.* 3(1973) 610–621.
- [9] E. Kyriakou, M.S. Pattichis, C. Christodoulou, C.S. Pattichis, S. Kakkos, M. Griffin, A.N. Nicolaides, Ultrasound imaging in the analysis of carotid plaque morphology for the assessment of stroke, in: J.S. Suri, C. Yuan, D.L. Wilson, S. Laxminarayan (Eds.), *Plaque Imaging: Pixel to Molecular Level*, IOS Press, Amsterdam, Netherlands, 2005, pp. 241–275.
- [10] J. Grosby, B.H. Amundsen, T. Hergum, E.W. Remme, S. Langland, H. Trop, 3D speckle tracking for assessment of regional left ventricular function, *Ultrasound Med. Biol.* 35(2009) 458–471.
- [11] J.A. Noble, N. Navab, H. Becher, Ultrasonic image analysis and image guided interventions, *Interface Focus* 1 (2011) 673–685.
- [12] C.P. Loizou, C.S. Pattichis, M. Pantziaris, T. Tyllis, A.N. Nicolaides, Quality evaluation of ultrasound imaging in the carotid artery based on normalization and speckle reduction filtering, *Med. Biol. Eng. Comput.* 44 (5) (2006) 414–426.
- [13] C.P. Loizou, C.S. Pattichis, A.N. Nicolaides, M. Pantziaris, Manual and automated media and intima thickness measurements of the common carotid artery, *IEEE Trans. Ultrason. Ferroelectr. Freq. Control* 56 (5) (2009) 983–994.
- [14] C.P. Loizou, C.S. Pattichis, M. Pantziaris, T. Tyllis, A.N. Nicolaides, Snakes based segmentation of the common carotid artery intima media, *Med. Biol. Eng. Comput.* 45 (1)(2007) 35–49.
- [15] C.P. Loizou, C.S. Pattichis, M. Pantziaris, A.N.

**International Journal of Engineering Research in Electronic and Communication Engineering
(IJERECE)
Vol 3, Issue 5, May 2016**

- Nicolaides, An integrated system for the segmentation of atherosclerotic carotid plaque, *IEEE Trans. Inform. Technol. Biomed.* 11 (6)(2007) 661–667.
- [16] C.P. Loizou, C. Theofanous, M. Pantziaris, T. Kasparis, P. Christodoulides, A.N. Nicolaides, C.S. Pattichis, Despeckle filtering toolbox for medical ultrasound video, *Int. J. Monitor. Surveillance Technol. Res. (IJMSTR)* 4 (1) (2014) 61–79, Oct.-Dec. 2013 (Special issue on Biomedical Monitoring Technologies).
- [17] C.P. Loizou, T. Kasparis, P. Christodoulides, C. Theofanous, M. Pantziaris, E. Kyriakou, C.S. Pattichis, Despeckle filtering in ultrasound video of the common carotid artery, in: 12th International Conference on Bioinformatics & Bioengineering Processing (BIBE), Larnaca, Cyprus, November 11–13, 2012, p. 4.
- [18] C.P. Loizou, M. Pantziaris, C.S. Pattichis, E. Kyriakou, M-mode state-based identification in ultrasound videos of the common carotid artery, in: Proceedings of 4th International Symposium on Communication Control & Signal Processing, ISCCSP, Limassol, Cyprus, March 3–5, 2010, p. 6.
- [19] C.P. Loizou, C.S. Pattichis, S. Petroudi, M. Pantziaris, T. Kasparis, A.N. Nicolaides, Segmentation of atherosclerotic carotid plaque in ultrasound video, in: 34th Annual International Conference on IEEE Engineering Medicine and Biology, EMBC, San Diego, USA, August 28–September 1, 2012, p. 4.
- [20] P.H. Davis, J.D. Dawson, M.B. Biecha, R.K. Mastbergen, M. Sonka, Measurement of aortic intimal-media thickness in adolescents and young adults, *Ultrasound Med. Biol.* 36 (4)(2010) 560–565.
- [21] E. Heiberg, J. Sjogren, M. Ugander, M. Carlsson, H. Engblom, K. Arheden, Design and validation of a segment-freely available software for cardiovascular image analysis, *BMC Med. Imaging* 10 (1) (2010) 1–13.
- [22] E.C. Kyriakou, C.S. Pattichis, M.A. Karaolis, C.P. Loizou, M.S. Pattichis, S. Kakkos, A.N. Nicolaides, An integrated system for assessing stroke risk, *IEEE Eng. Med. Biol. Mag.* 26 (5)(2007) 43–50.
- [23] F. Molinari, K.M. Meiburger, J. Suri, Automated high-performance cIMT measurement techniques using patented AtheroEdge™: a screening and home monitoring system, in: 33rd Annual International Conference on IEEE EMBS, Boston, USA, 2011, pp. 6651–6654.
- [24] X.G. Xu, Y.H. Na, T. Zhang, Design and test of a PC-based 3D ultrasound software system Ultra3D, *Comp. Biol. Med.* 38 (2) (2008) 244–251.
- [25] R. Cardenas-Almeida, A. Tristan-Vega, G.V.-S. Ferrero, S.A. Fernandez, et al., Usimagtool: an open source freeware software for ultrasound imaging and elastography, in: International Work on Multimodal Interfaces, eINTERFACE, Istanbul, Turkey, 2007, pp. 117–127.
- [26] J.S. Lee, Digital image enhancement and noise filtering by using local statistics, *IEEE Trans. Pattern Anal. Mach. Intell. PAMI-2 2* (1980) 165–168.
- [27] V.S. Frost, J.A. Stiles, K.S. Shanmungan, J.C. Holtzman, A model for radar images and its application for adaptive digital filtering of multiplicative noise, *IEEE Trans. Pattern Anal. Mach. Intell.* 4 (2) (1982) 157–165.
- [28] M. Kuwahara, K. Hachimura, S. Eiho, M. Kinoshita, in: K. Preston, M. Onoe (Eds.), *Digital Processing of Biomedical Images*, Plenum Publishing Corporation, New York, 1976, pp. 187–203.
- [29] L.J. Busse, T.R. Crimmins, J.R. Fienup, A model based approach to improve the performance of the geometric filtering speckle reduction algorithm, in: *IEEE Ultrasonic Symposium*, 1995, pp. 1353–1356.
- [30] A. Nieminen, P. Heinonen, Y. Neuvo, A new class of detail-preserving filters for image processing, *IEEE Trans. Pattern Anal. Mach. Intell.* 9 (1987) 74–90.
- [31] P. Perona, J. Malik, Scale-space and edge detection using anisotropic diffusion, *IEEE Trans. Pattern Anal. Mach. Intell.* 12 (7) (1990) 629–639.
- [32] A. Panayides, M.S. Pattichis, C.S. Pattichis, C.P. Loizou, M. Pantziaris, A. Pitsillides, Atherosclerotic plaque ultrasound video encoding, wireless transmission, and quality assessment using H.264, *IEEE Trans. Inform. Technol. Biomed.* 15 (3) (2001) 387–397.
- [33] Y. Yongjian, S.T. Acton, Speckle reducing anisotropic diffusion, *IEEE Trans. Image Process.* 11 (11) (2002) 1260–1270.
- [34] A Philips medical system company, Comparison of image clarity, SonoCT Real-time Compound Imaging Versus Conventional 2D Ultrasound Imaging, ATL Ultrasound Report, 2001.
- [35] A.N. Nicolaides, M. Sabetai, S.K. Kakkos, S. Dhanjil, T. Tegos, J.M. Stevens, The asymptomatic carotid stenosis and risk of stroke study, *Int. Angiol.* 22 (3) (2003) 263–272.
- [36] J.S. Weszka, C.R. Dyer, A. Rosenfield, A comparative

**International Journal of Engineering Research in Electronic and Communication Engineering
(IJERECE)
Vol 3, Issue 5, May 2016**

- study of texture measures for terrain classification, *IEEE Trans. Syst. Man Cybernet.* 6 (1976) 269–285.
- [37] M. Amadasun, R. King, Textural features corresponding to textural properties, *IEEE Trans. Syst. Man Cybernet.* 19 (5) (1989) 1264–1274.
- [38] D.G. Altman (Ed.), *Practical Statistics for Medical Research*, Chapman & Hall, London, 1991.
- [39] C.P. Loizou, T. Kasparis, P. Papakyriakou, L. Christodoulou, M. Pantziaris, C.S. Pattichis, Video segmentation of the common carotid artery intima-media complex, in: *12th International Conference on Bioinformation & Bioengineering Process (BIBE)*, Larnaca, Cyprus, November 11–13, 2012, p. 4.
- [40] V. Zlokolica, W. Philips, van de Ville, Robust non-linear filtering for video processing, *IEEE Proc. Vision Imag. Signal. Process.* 2 (2) (2002) 571–574.
- [41] V. Zlokolica, A. Pizurica, W. Philips, Recursive temporal denoising and motion estimation of video, *Int. Conf. Image Process.* 3 (3) (2008) 1465–1468.
- [42] E. Brusseau, C.L. De Korte, F. Mastick, J. Schaar, A.F.W. van der Steen, Fully automatic luminal contour segmentation in intracoronary ultrasound imaging – a statistical approach, *IEEE Trans. Med. Imaging* 23 (5) (2004) 554–566.
- [43] J.A. Noble, A. Boukerroui, Ultrasound image segmentation: a survey, *IEEE Trans. Med. Imaging* 25 (8) (2006) 987–1010.
- [44] A. Fenster, A. Zahalka, An automated segmentation method for three-dimensional carotid ultrasound images, *Phys. Med. Biol.* 46 (2001) 321–342.
- [45] L. Chrzanowski, J. Drozd, M. Strzelecki, M. Krzeminska-Pakula, K.S. Jedrzejewski, J.D. Kasprzak, Application of neural networks for the analysis of intravascular ultrasound and histological aortic wall appearance – an in vitro tissue characterisation study, *Ultrasound Med. Biol.* 34 (1) (2008) 103–113.
- [46] M. Strzelecki, P. Szczypinski, A. Materka, A. Klepaczko, A software tool for automatic classification and segmentation of 2D/3D medical images, *Nucl. Instrum. Method Phys. Res.* 702 (2013) 137–140.
- [47] A.M.F. Santos, R.M. Dos Santos, P.M.A. Castro, E. Azevedo, et al., A novel algorithm for the segmentation of the lumen of the carotid artery in ultrasound B-mode images, *Expert Syst. Appl.* 40 (2013) 6570–6579.
- [48] K. Potter, D.J. Green, C.J. Reed, R.J. Woodman, et al., Carotid intima-media thickness measured on multiple ultrasound frames; evaluation of a DICOM-based software system, *Cardiovasc. Ultrasound* 5 (29) (2007) 1–10.
- [49] P.M. Szczypinski, M. Strzelecki, A. Materka, A. Klepaczko, MaZda – a software package for image texture analysis, *Comp. Methods Prog. Biomed.* 94 (1) (2008) 66–76.